



# **Summer Student project report: counting antiprotons in ASACUSA's Cusp trap**

Author: Michael Cripe

Supervisors: Eric Hunter and Marcus Bumbar

September 13, 2024

## **1 Introduction**

Antimatter is an elusive part of our universe, but its understanding is crucial to the development of coherent and well functioning theories. It was first discovered in the 20th century, and its existence was predicted by the physicist Paul Dirac. The most common way to obtain antimatter is through  $\beta$  decay, where a proton will decay into a neutron, a positron as well as a neutrino  $p \rightarrow n + \beta^+ + \nu_e$ . The positron is the first antimatter particle to be discovered, which occurred in 1932 by Carl Anderson. To make more complex antimatter structures, large machinery is required. In particular, accelerators are necessary. This allows us to collide charged particles with a target, selecting for a precise reaction yielding the desired antimatter. At CERN, this happens in the antimatter factory [1,2], where protons from the Proton Synchrotron are collided with an iridium target to produce antiprotons. Once produced, they can be stored and various properties can be studied. In particular, the ASACUSA collaboration is working towards measuring the hyperfine structure of antihydrogen. To do so, it is crucial to have an estimation of how much antimatter was trapped for a given experiment. This leads to the subject of this report, which concerns some of the antimatter detectors in the ASACUSA collaboration. Firstly, antiproton plasma was dumped onto a microchannel plate-phosphor screen (MCP) detector outside the trap, with the emitted light being recorded by two independent silicon photomultiplier (SiPM) systems. The results were analyzed and compared to control for systematic effects in identifying single annihilation events. Secondly, antiprotons were caused to annihilate inside the trap, at a magnetic field minimum. The annihilation signal was recorded by a scintillator bar system, which is connected to photomultipliers (PMTs). This system also needs to have its efficiency estimated. To do so, simulations were conducted and analyzed. The ultimate goal was to study these reliability of the detectors of the ASACUSA experiment and characterize their behavior to make better estimates of the amount of antiprotons that are being trapped.

## **2 Experimental Setup & Procedure**

### **2.1 MCP and SiPM detectors**

Antiprotons are slowly released from ASACUSA's Cusp trap so that they impact the MCP, and the light is detected by two SiPMs, similar to Ref. [3]. The linear signal of the first SiPM (called "slow SiPM") is sampled at a frequency of 5 MS/s, and the maximum acquisition time is 100 ms. The pulses from the waveform are around 5  $\mu$ s wide, therefore we extract over 100 s to keep the pulses separated such that they can be resolved. It is not possible for us to sample at 5 MS/s over 100s, therefore NIM electronics must be used to convert the signal from the other SiPM (called "fast SiPM") to counts.

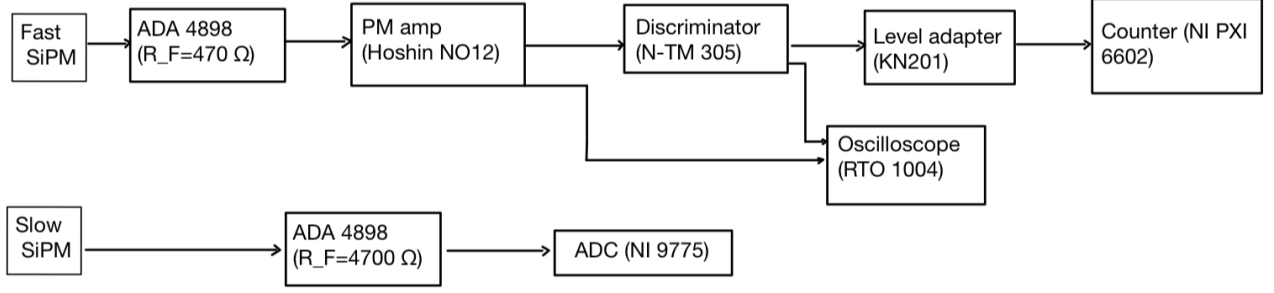


Figure 1: Schematic of the SiPM detector setup.

There are 2 possible procedures to benchmark this conversion: first, the fast SiPM counts can be compared to our own analysis of the full signal from the slow SiPM for a few hundred small samples (called "scoops") from an antiproton plasma reservoir; second, it is possible to compare the fast SiPM counts to our own analysis of the fast SiPM signal during the slow extraction, over a 200 ms windows, by sampling both with the oscilloscope. There are many peaks in intensities in the waveform packets that are received. The smallest ones are not the result of antimatter annihilations and therefore must be discarded when considering the counts of the detector. To do this, a threshold tension  $\epsilon$  [V] was chosen in order to determine when a peak corresponds to an annihilation. Then, the peaks corresponding to the desired interactions were summed up to count the total amount of antimatter present in a given cycle and compared to the counts from the fast SiPM detector. It was suspected that the fast detector should pick up more counts. This is due to the fact if there several annihilations that occur in rapid succession, the slow detector will identify one large peak, whereas the fast one should pick up each peak individually. In fact, as shown in Fig. 2, the pulse width of the fast detector after amplification is about the same as that of the slow detector.

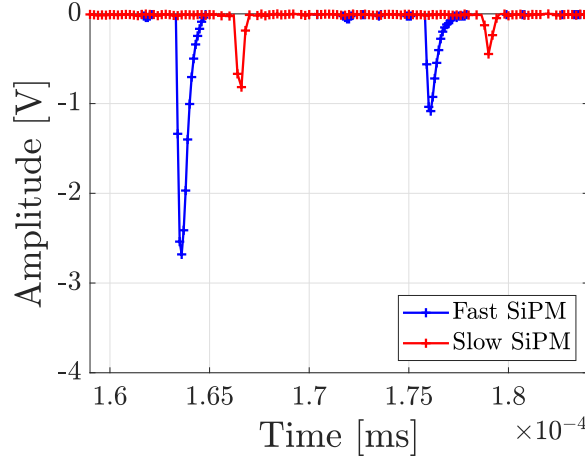


Figure 2: Examples of pulses for the fast SiPM detector and slow SiPM detector.

A pulse height histogram was done with the data from the slow SiPM in order to determine a proper threshold value to apply the counting algorithm to. In parallel, the threshold tension was varied in order to see what ranges yielded more and fewer counts to the slow SiPM with respect to the fast SiPM. Then, a threshold tension was set, and the counts from both detectors were compared, first over time as the  $\bar{p}$  was dumped in scoops towards the MCP, then in a scoop by scoop fashion. Finally, the discriminator algorithm implemented for the slow SiPM was used on the fast SiPM in order to compare with the output of the electronic discriminator.

## 2.2 AMT Scintillator

The ASACUSA collaboration also has scintillating bar detector system, formerly used to trigger the ASACUSA Micromegas Tracker (AMT) [4]. Unlike the MCP-SiPM system, the AMT scintillator may only detect a small fraction of antiproton annihilations. Thus, it requires careful modeling to convert from AMT events to the total number of antiprotons. To study this detector, the results from simulations conducted by Viktoria Kraxberger using the program FLUKA [5] were manipulated. In these simulations, antiprotons were annihilated at various positions along the axis of the trap. A total number of 1'000 or 10'000 particles were annihilated at each position. These annihilations would produce particles that deposit energy along the the scintillator panels or on the trap walls.

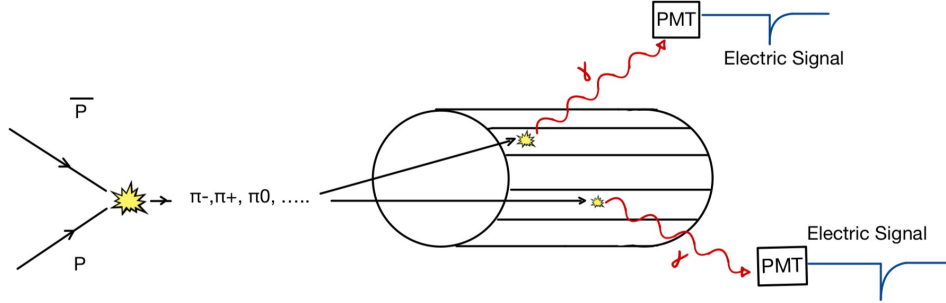


Figure 3: Physical process of  $\bar{p} + p$  annihilating being simulated in FLUKA.

The energy, annihilation position, and time among other variables were simulated for each event, which represents 1 antiproton annihilating, and therefore producing multiple secondary particles. With this information, the first step was to select the events where a particle deposited energy in one of the 8 scintillator panels. To do so, a constraint was applied to the axial position of the event, the distance to the center of the trap as well as whether they hit the wall or the scintillator panels. Then, for each event, the energy deposited in each panel was added up. In order to determine if the  $\bar{p}$  annihilation deposited enough energy in the panels to create a flash of light that could be picked up by the photo multipliers, an energy threshold needed to be set. As a first step, this value was set to the first quartile of the energy deposits. The coincidences were then calculated, first a simple 2 and 3 coincidence counter was setup, meaning if at least 2 or three panels light up respectively, 1 coincidence is measured. This allowed a preliminary estimate of the efficiency to be obtained. Then, the coincidence counters were calculated according to how the experimental setup can count coincidences. The PMT system is equipped with a discriminator, whose signals then pass into a comparator. This comparator can only take as an input 1 signal to be compared to the other inputs. Meaning, it is only possible to do some combination of channel X and the others (e.g  $\text{ch X} \wedge \text{ch Y} \vee \text{ch Z}$ ). As it stands now, channel 1 is used for this purpose. This counting method was combined with the results from the FLUKA simulations to scan the energy threshold. The corresponding coincidence logics were implemented in the PMT setup and the counts were recorded for the given logic as well as the counts in channel 1. This is so that the coincidence counts, measured or simulated can be normalized to the counts of channel 1. One set of 3 measurements were taken for each channel logic for a common discriminator threshold tension of -150 mV. Using the three measurements for each coincidence logic (both normalized to channel 1), the intersection points between the

coincidence curves from FLUKA and the corresponding horizontal measurement lines could be determined. This yields the energy threshold corresponding to the discriminator threshold in the setup. Using the former, the coincidence counts at the given value were taken and divided by the total number of simulated particles thus giving a more precise estimate of the efficiency. As an extra step, to verify that the energy threshold corresponds to the threshold tension on the discriminator, positrons were simulated in FLUKA and stacked in the cusp, where their annihilation counts were measured. The energy spectrum of positrons is relatively simple and more well known. Therefore it can be used to better calibrate the PMT response for a given energy deposit. This is important due to the fact that the PMTs of each channel don't send the same electrical signal amplitude for the same energy deposited. In other words, they have different sensitivities, where sensitivity can be defined as :

$$Sensitivity = \frac{PMT\ peak\ height}{Energy\ deposited\ in\ 1\ AMT\ panel} \quad (1)$$

with sensitivity ration defined as:

$$Sensitivity\ ratio = \frac{threshold\ for\ x\ counts\ in\ each\ channel}{150\ mV} \quad (2)$$

with  $x\ counts$  being determined by the number of counts in channel 1 at -150 mV discriminator threshold.

### 3 Results

#### 3.1 MCP and SiPM detectors

The first step in analyzing the efficiency of the slow SiPM detector was to determine a good threshold tension. If the threshold is too high, annihilations would be missed, falsifying the readout. If the threshold is too low, it could count interactions of other particles or background noise which is undesirable. Therefore, a peak height histogram was made to determine what tension region would be physically reasonable to select the threshold value. The resulting histogram is shown in the figure below Fig:4.

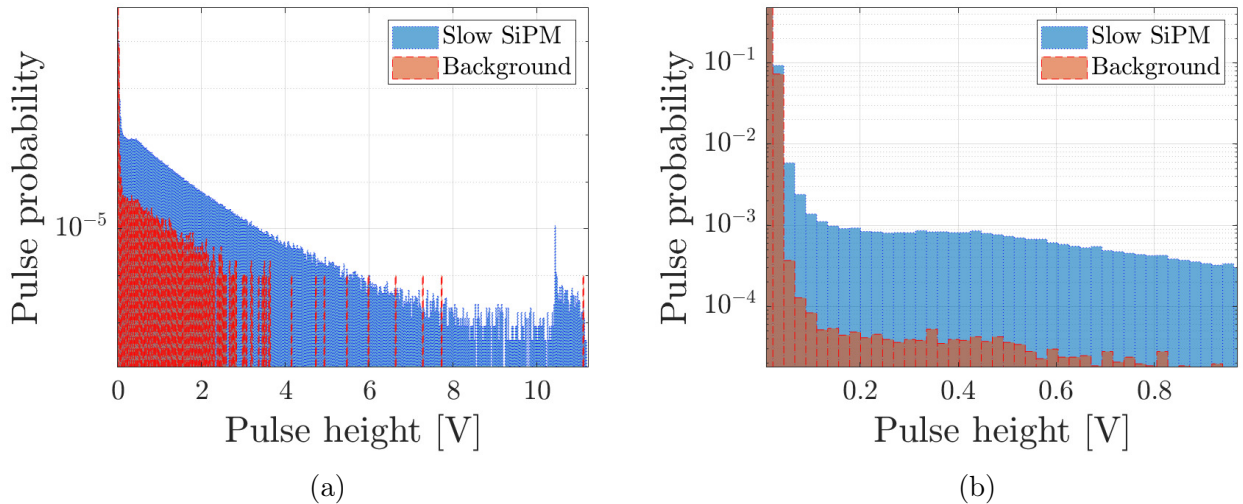


Figure 4: Pulse height vs tension range histogram with the SiPM pulses (blue) and background pulses (red), a) the complete histogram, b) a zoomed area where the signal to noise ratio rises.

The results were normalized to give a probability distribution, with the  $y$  axis plotted in a log scale for visibility reasons.

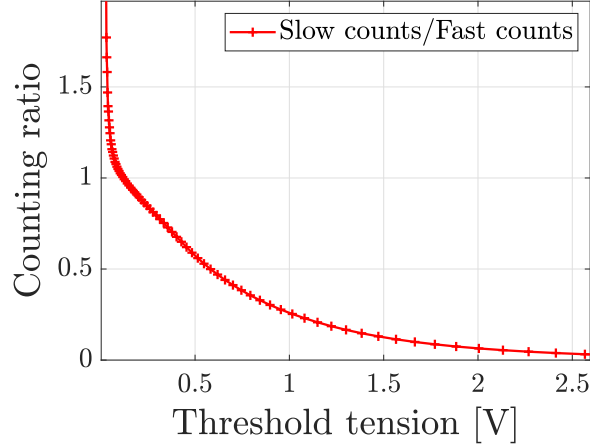


Figure 5: Total counts versus threshold tension normalized with respect to the counts from the slow SiPM.

It is also interesting to observe the total counts in the slow SiPM as a function of the threshold tension. This is shown in the previous figure Fig:5. The background was subtracted from the total number of counts, which was then normalized to the counts from the fast SiPM. The background counts were obtained by counting the peaks in an area of the waveforms where there was no antimatter being sent towards the MCP. These were then adjusted to be representative of the background included in the area where there was signal. With the histogram and the threshold tension scan, the threshold  $\epsilon$  was set to 0.1 V. The data from the both SiPM were then analyzed and are presented in the following figures.

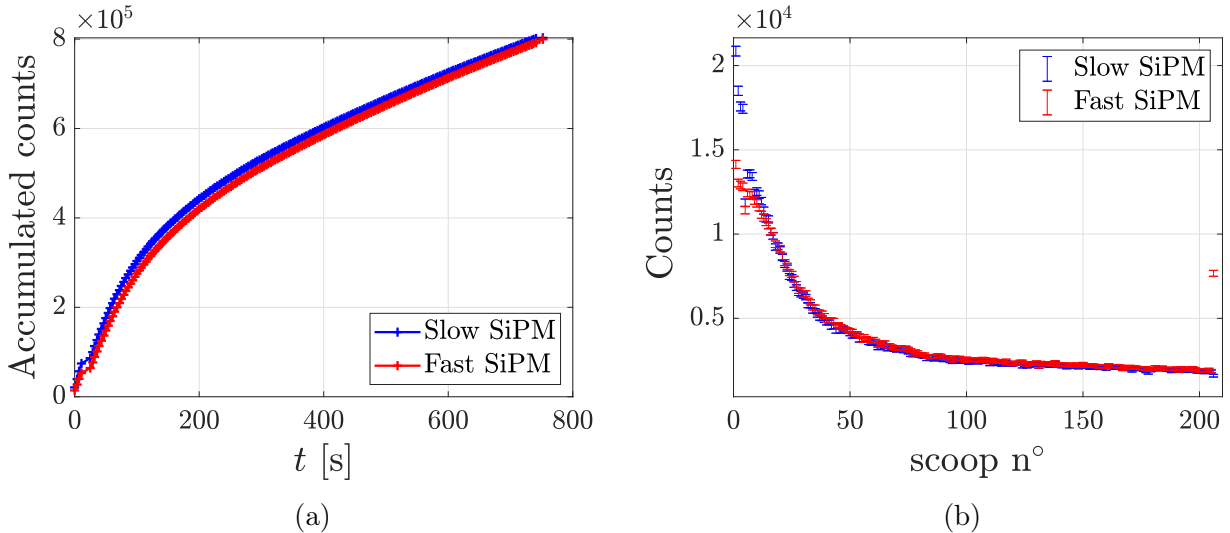


Figure 6: Counts from the fast and slow SiPMs, a) total counts over time, b) counts for each scoop.

The signal from the fast SiPM can also be obtained as a waveform. This signal can be compared to itself after having been passed through the discriminator in order to make a comparison with the algorithm implemented for the slow SiPM. The MCP gain was varied from 800 V to 900 V and finally to 1000 V, and the waveforms were taken in a few isolated

200 ms windows during a 100 s extraction of  $\bar{p}$  to the MCP. First, the discriminated signal was verified that it picked up the correct pulses from the MCP, then the counts from both signals were compared as a function of discriminator threshold. These results are presented in the figure below.

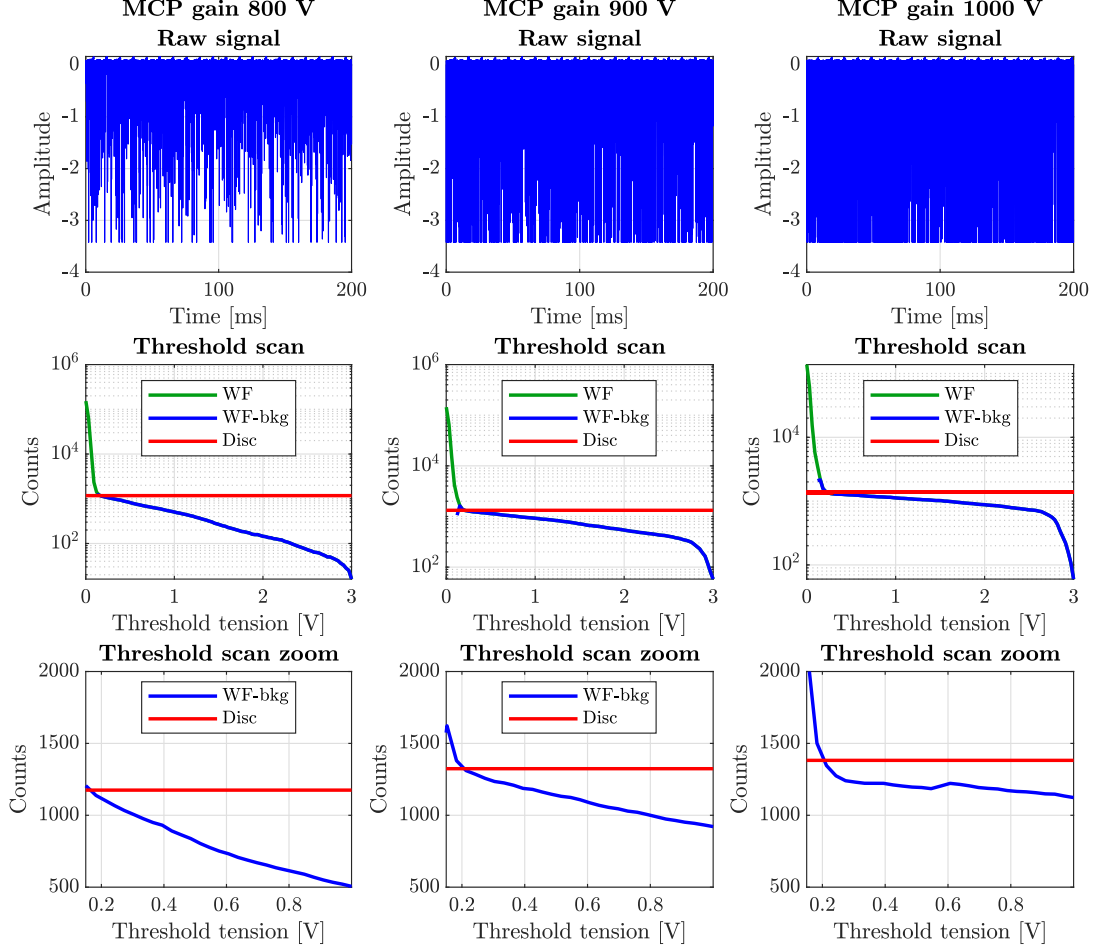


Figure 7: MCP gain variation : 1st column MCP gain 800 V, 2nd column MCP gain 900 V, 3rd column MCP gain 1000 V, 1st line waveform signal from fast SiPM, 2nd line counts from the waveform signal as a function of threshold tension with discriminator counts, 3rd line a zoomed area of the previous plot showing the crossing of the 2 curves.

### 3.2 AMT Scintillator

The events of interest occur in the scintillator panels, therefore a radial constraint must be applied. As a first step, it is interesting to analyze where most particles deposit their energy and to check if this corresponds to the position of the scintillator panels. The output of the FLUKA simulations gives various properties of the events, such as position, medium, and energy deposited to name a few. The medium can be one of two options: 'void' or 'scintillator'. A histogram of the radial distribution of events, as well as a histogram after removing the events that occurred outside of the cusp, are presented in the next figures. This was done by removing all of the events with an event medium labeled 'void'.

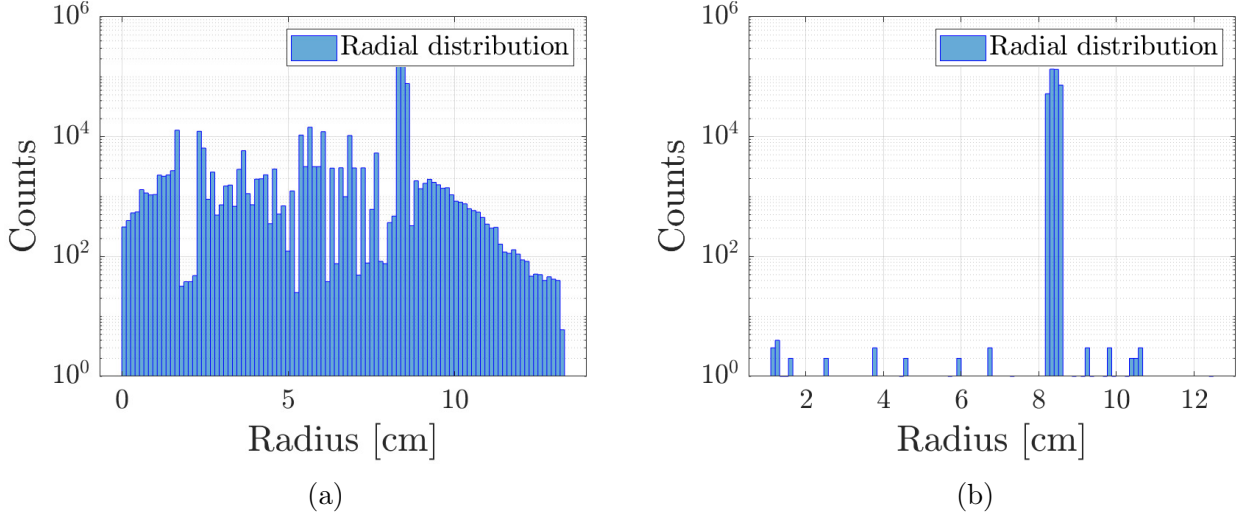


Figure 8: Radial distribution of events, a) before removing events outside of the cusp, b) after removal.

Next, the angular distribution needed to be determined in order to calculate how much energy was deposited in each panel. This distribution is shown in the figure below.

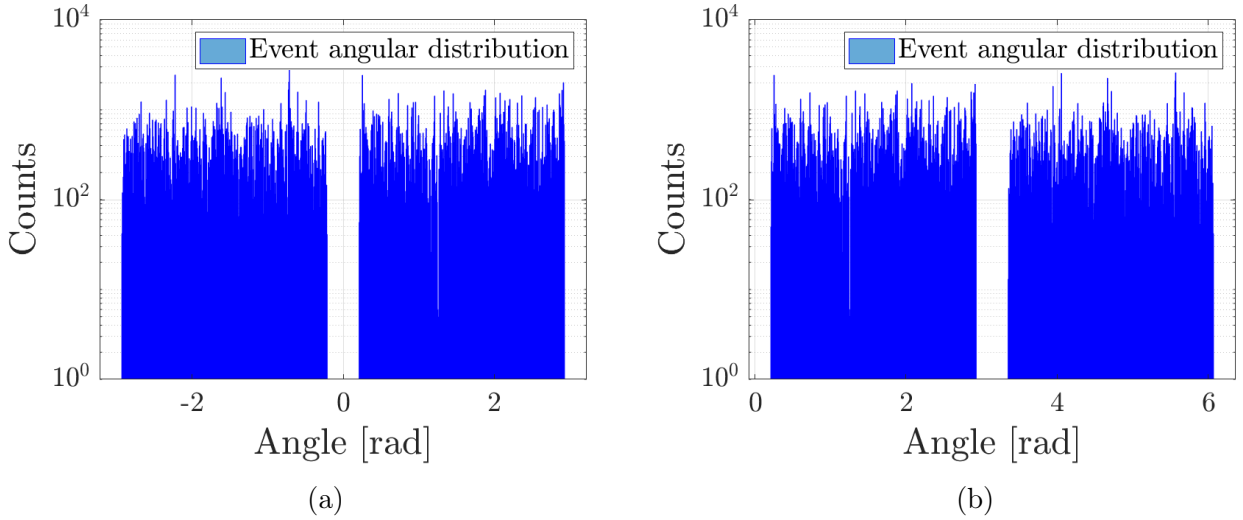


Figure 9: Angular distribution of events, a) full range, b) modulo  $2\pi$ .

With these steps completed, the counting efficiency of the AMT was estimated for each region of the cusp. The initial number of  $\bar{p}$  is known, therefore by dividing the number of coincidences by this number, it is possible to estimate the efficiency. The coincidences are counted either as 2, meaning if 2 panels light up that makes up one coincidences, or 3, where at least 3 panels light up to make a coincidence. Depositing energy in a panel alone is not sufficient to make a flash that can be picked up by the PMT's. There needs to be a minimal amount of energy to create a burst of light. As a first run, this minimal energy was considered to be the first quartile. The 2 and 3 coincidence efficiencies are presented in the figure below, as well as the ratio between the 2 and 3 coincidence efficiencies as a function of the set energy threshold.



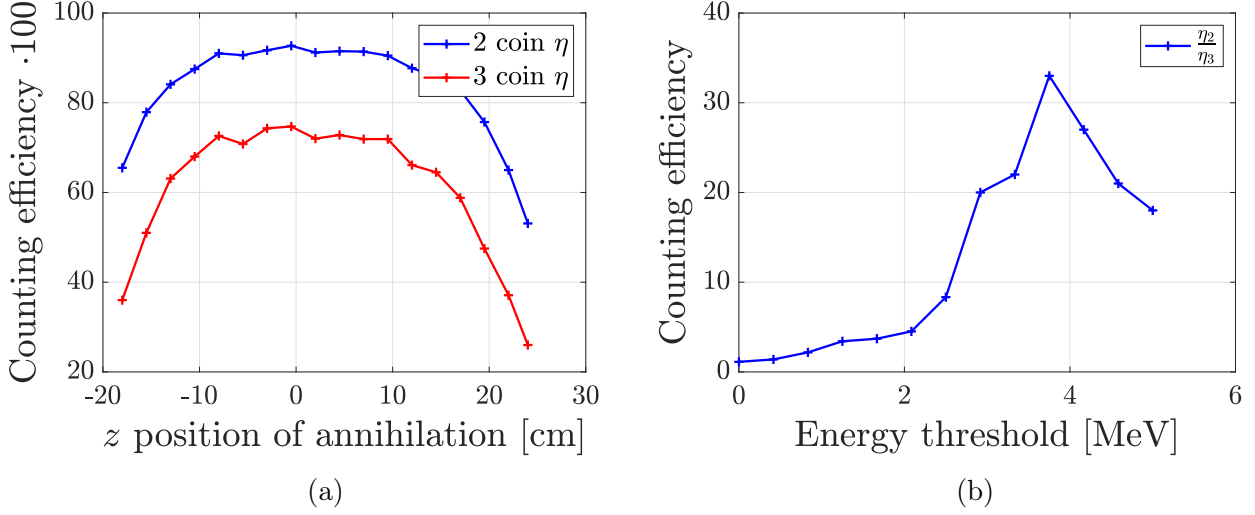


Figure 10: Coincidence efficiencies, a) 2 and 3 coincidence vs  $z$  position of annihilations, b) efficiency ratio at  $z = 0$  vs energy threshold.

From figure Fig:10a, it seems as though the highest efficiency is around  $z = 0$ , which corresponds to the field null in the cusp. This efficiency can be studied with respect to the energy threshold that is set. With experimental data, it is possible to obtain the corresponding energy threshold of the actual AMT panels. In the figure below, the energy threshold scan is shown in terms of a linear interval of thresholds as well as a logarithmic interval. This choice of interval was done in order to ensure no behavior was missed while keeping the number of points to scan minimal to maintain a reasonable computing time.

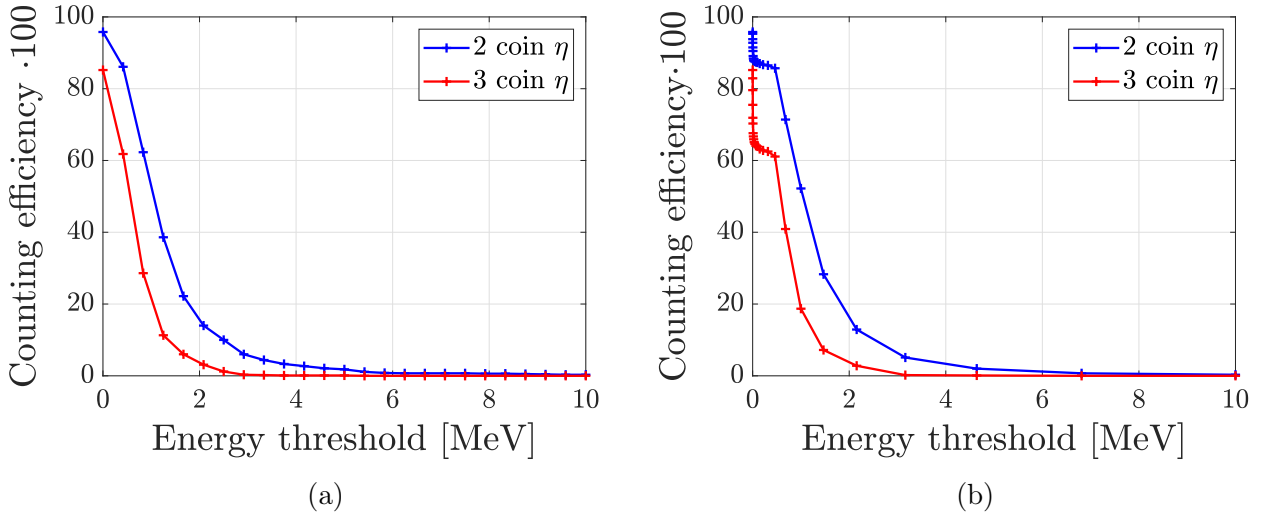


Figure 11: AMT energy threshold scan, a) linear energy interval, b) logarithmic energy interval.

To estimate the efficiency of the detector, measurements were taken at a certain discriminator threshold, with a coincidence logic (e.g  $\text{ch1} \&\& \text{ch2}||\text{ch3}$ ), along with the counts in channel 1. This allows the coincidences to be normalized with respect to the counts of channel 1. This yields multiple horizontal lines that when taking the intersection point between our simulations and the measurements give the corresponding energy threshold, effectively converting Volts to eV. This was done for various logic configurations combining channel 1 and some combination of the remaining channels. The results are plotted in the figures below.



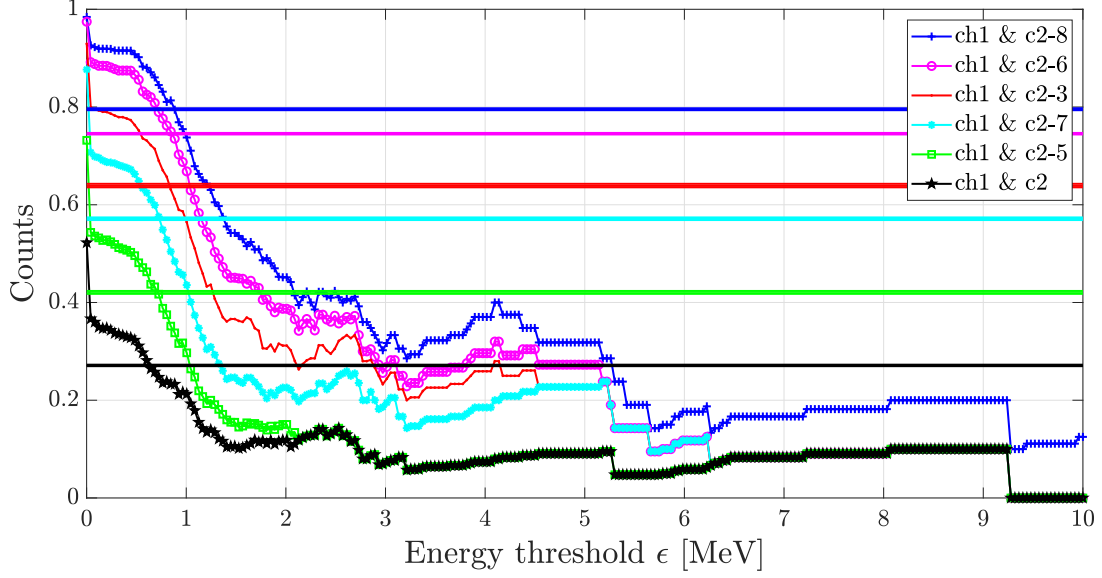


Figure 12: Simulated coincidence logic counts normalized to the counts from channel 1 with measured data, as well as simulated data. The horizontal lines, which correspond to the measured data, of the same color as the curve correspond to the same coincidence logic.

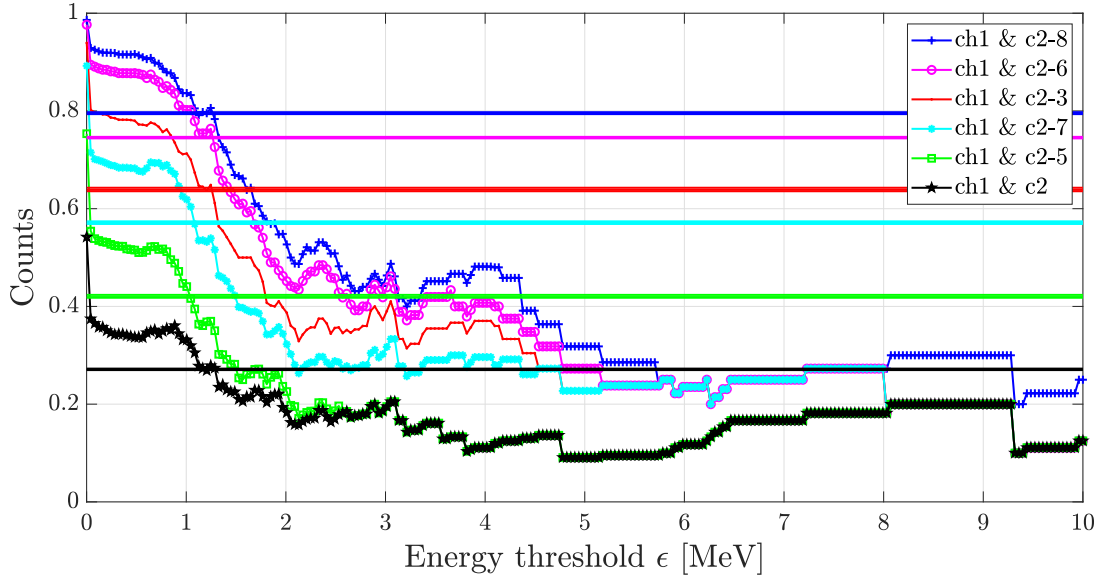


Figure 13: Simulated coincidence logic counts normalized to the counts from channel 1 with measured data, as well as simulated data corrected for sensitivity (see eq:2).

The configuration maximizing the counts is the one of interest in this report, which is  $(ch1 \wedge (ch2 \vee \dots \vee ch8))$ . The results for the coincidence logic of channel 1 and any of the remaining 6 channels are plotted in the figure below, along with the simulated coincidence trend for all the available configurations.

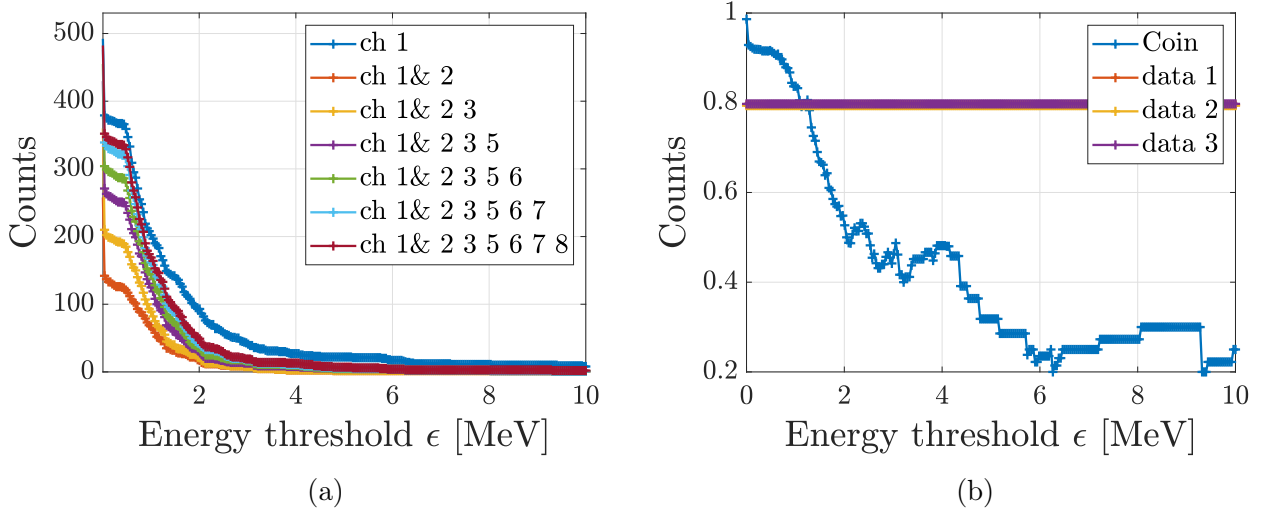


Figure 14: Coincidence logic counts, a) all possible configurations, b) channel 1 and any of the remaining available channels with measured data.

The horizontal lines, being the measured data divided by the counts in channel 1, intersect the simulated normalized coincidence counter at the energy threshold that corresponds to the discriminator threshold. Using these intersection points for the maximal coincidence count configuration, it is possible to estimate the efficiency. This is done by taking the counts at the previously found threshold and dividing them by the total number of particles. These results are presented in the figure below for channel 1 and any of the others, as well as channel 1 on its own.

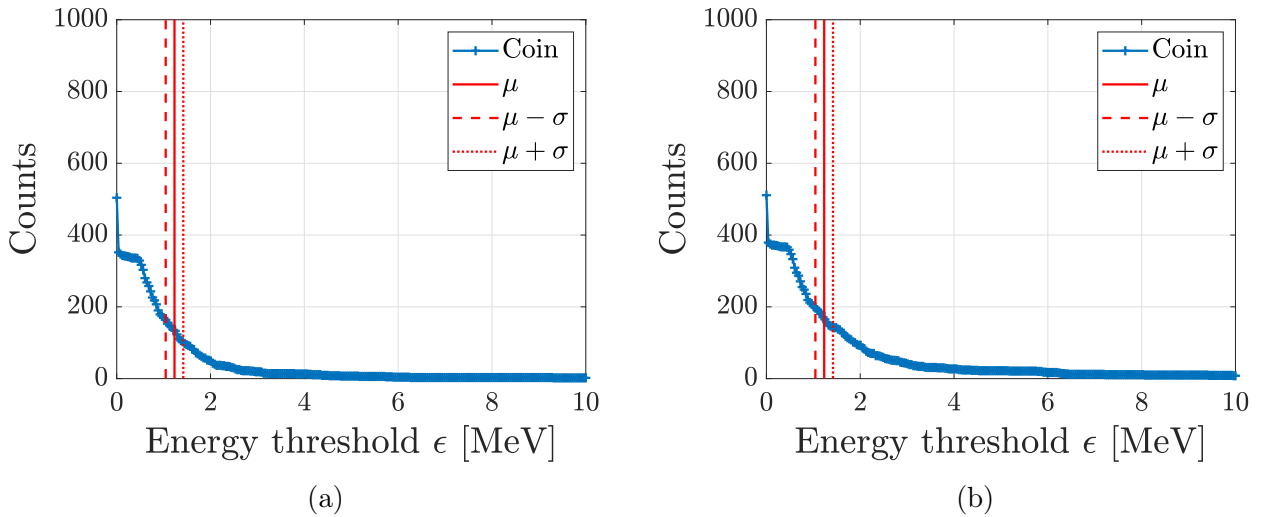


Figure 15: Efficiency estimates for 2 logic configurations, a) (ch1 && (ch2||...||ch8)), b) channel 1.

For the measurements with positrons, the discriminator thresholds were set to the same value which was varied between -325 mV and -15mV. This was done in an attempt to determine the energy spectrum of positron annihilations. At certain tensions, multiple measurements were done to roughly estimate the uncertainty. The results of these measurements are presented in the figure below along with the error-bars where available.

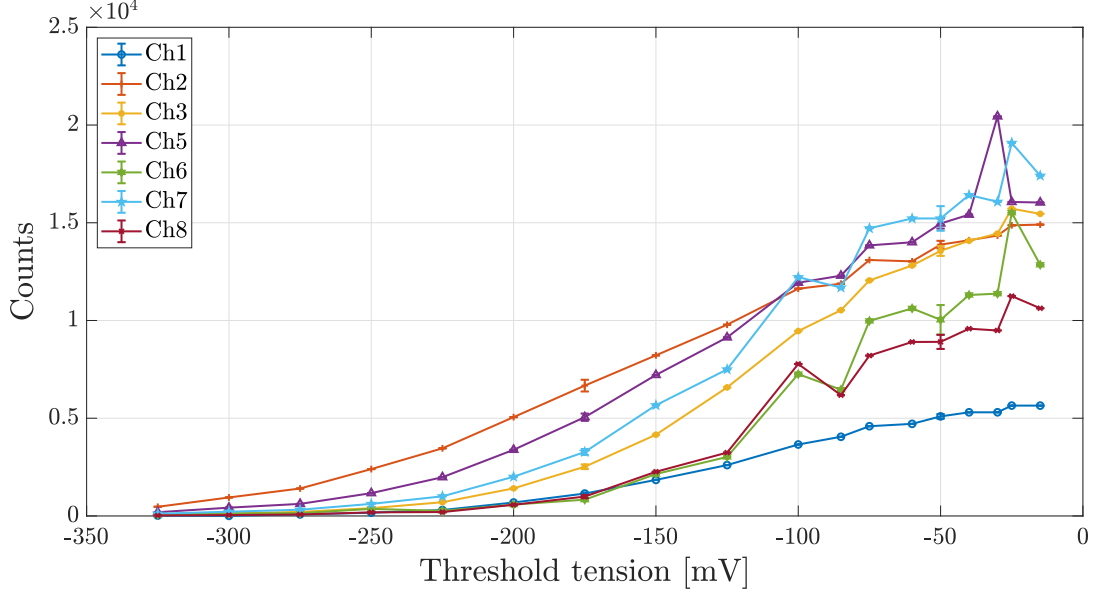


Figure 16: Positron annihilation counts in each panel vs discriminator threshold.

Using equation eq:2 as well as the results above, it is possible to estimate the sensitivity of each channel and subsequently correct the coincidence counts accordingly. This is how the results differ in figure Fig:12 & Fig:13.

In FLUKA, the simulations were set to generate between 10'000 and 50'000 positrons. Initially, the geometry of the simulation input matched that of the actual scintillating bar. However, 511 keV photons were not present in the results. Therefore the thickness of the scintillating bar was changed until these gamma rays could be detected. The total number of counts of each channel were added up and then divided by 8 to obtain an average count rate at a given threshold. The output of these operations is presented in the figures below:

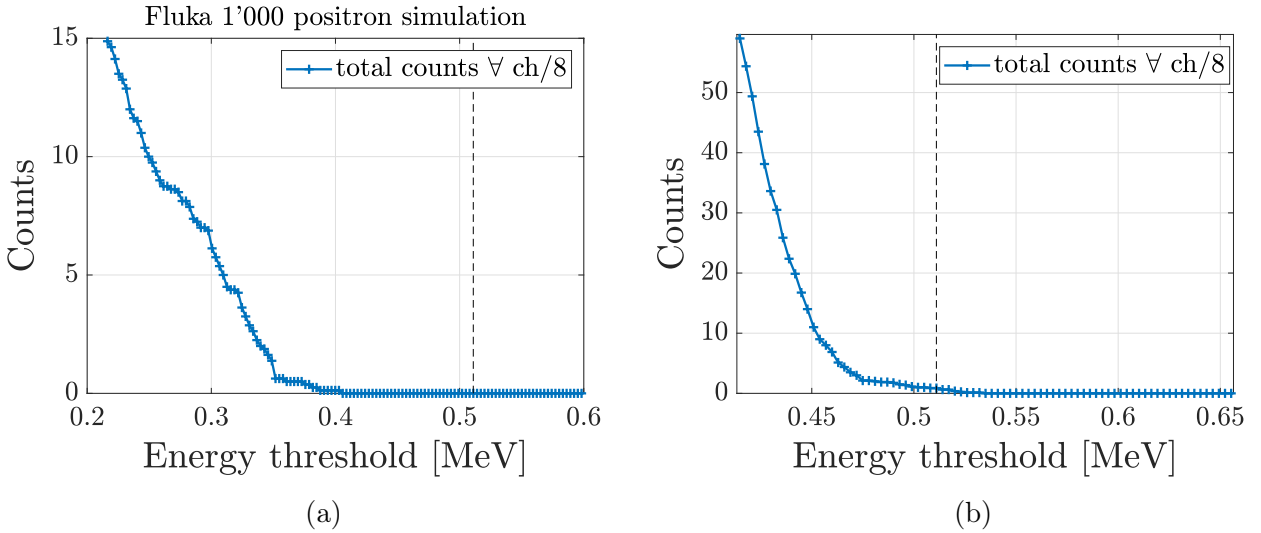


Figure 17: Average annihilation counts over all channels from Fluka simulations, a) 10'000 positrons with original geometry, b) of 50'000  $e^+$  with 8X thicker scintillating bar.

### 3.3 Estimated quantity of $\bar{p}$

With the efficiencies obtained above, it is possible to estimate the amount of  $\bar{p}$  held within the cusp or reservoir. These estimates are presented in the table below, along with the date when the measurements were taken. This last point is important to consider because we weren't always catching the same amount of  $\bar{p}$  over the course of this project, due to factors beyond our control.

Table 1: Values of the amount of  $\bar{p}$  trapped in the experiment

System	Fast SiPM	Slow SiPM	AMT ch1	AMT coincidence
In this document	Fig. 7	Fig. 6	Fig. 15	Fig. 15
Date of acquisition	03.09.2024	11.07.2024	03.09.2024	03.09.2024
Estimated quantity	$(1.41 \pm 0.17) \cdot 10^6$	$(8.1 \pm 0.3) \cdot 10^5$	$(9 \pm 1) \cdot 10^5$	$(9 \pm 2) \cdot 10^5$

## 4 Discussion

**MCP and SiPM detectors** From the histograms in the previous section, Fig:4a & Fig:4b, it can be seen that the signal to noise ratio for the slow SiPM drops considerably after 0.1 V. In this region, there are acceptable values of threshold tension that yield higher and lower counts than the fast SiPM. As of yet, physical grounds are missing that would allow a precise threshold tension to be set which would give more counts to the slow SiPM. Therefore, as a preliminary step, the threshold tension was set to 0.1 V. With this tension being set, the counts of each SiPM were obtained, first the accumulated counts, then the counts for each scoop. In the figure Fig:5, it is shown that the Slow SiPM counts surpass the fast SiPM counts in the signal to noise ratio drop off region, but as stated previously, there is a lack of physical grounds to set the threshold scan to yield more or less counts than the fast counter. In the accumulated scoops, it can be seen in figure Fig:6a that the fast SiPM initially sees more annihilations, but with time the two detectors seem to agree with the total counts. In the counts per scoop, it is possible to get an insight as to why that is. In figure Fig:6b, it can be seen that the first scoops yield far more counts, almost a factor of 2 more, in the fast SiPM than the slow. This could be due to the fact that the first scoops hold more  $\bar{p}$  as the reservoir is more full, causing pileup in the slow SiPM. As time progresses and the scoops contain fewer  $\bar{p}$ , the slow SiPM seems to have a greater sensitivity, until the last scoop where the remaining  $\bar{p}$  are all dumped towards the MCP and the slow detector can't keep up. Since it is considered that the dumping of  $\bar{p}$  is slow enough so that the slow SiPM can detect the signals from the annihilations, the total counts from the slow SiPM is used as a reference value. This allows the efficiency of the fast SiPM to be preliminarily estimated, which yields an efficiency of 99.5%. The uncertainty in this value has not yet been estimated, due to the fact that the background subtraction could be more rigorous, and the threshold on the slow SiPM was chosen in part arbitrarily to maximize counts while minimizing noise. Moreover, the uncertainty in the number of counts for a single scoop is not well known. The detectors follow a poisson distribution for the number of counts, as such the uncertainty in the counts per scoop was taken to be the square root of the counts. This estimation must still be verified.

The figure Fig:7 shows the linear signal plotted in 3 instances according to MCP gain, as well as the threshold tension scan on the signals with the discriminated counts in a horizontal plot. The counts from the discriminator intersect the threshold scan around 0.2 V, which is

what we expected given the way we took our measurements (1M $\Omega$  on the oscilloscope). What's interesting to note, is the counts curve flattens out more after this 0.2 V threshold as the MCP gain increases, meaning the discriminator counts are more reliable for higher MCP gain.

**AMT Scintillator** From the radial distribution histograms, figures Fig:8a & Fig:8b, it can be noted that there is a peak at a distance of approximately 8.5 cm from the center of the cusp. This peak is first seen in figure Fig:8a, which reaches orders of magnitude higher than the rest of the events. This peak remains after removing the events that occurred outside of the cusp, as can be seen in figure Fig:8b. This falls in accordance with the actual setup, where the scintillator panels are at a distance of 8.5 cm from the center of the cusp. The angular distribution was also analyzed, and is shown in figures Fig:9a & Fig:9b. These figures reveal that the gaps are between  $[-0.21, 0.21]$  and  $[2.9, 3.4]$  radians, which correspond to the actual setup. In figure Fig:10a, the 2 & 3 coincidence efficiencies are plotted against the  $z$  position of annihilation in the cusp. The trend shown in this figure is that the maximal efficiency is reached at a  $z = 0$  which corresponds to the field null of the cusp. At the field null, the 2 & 3 coincidence efficiencies are of 95% and 78% respectively. This was done by setting the energy threshold to be the value of the first quartile. In figure Fig:10b, the coincidence efficiency ratio  $\frac{\eta_2}{\eta_3}$  is plotted as a function of the energy threshold. This figure seems to suggest the highest efficiency ratio is obtained at a threshold value of 3.8 MeV.

The dependence of the coincidence efficiency on the energy threshold was studied and is presented in figures Fig:11a, where the energy thresholds are logarithmically spaced, & Fig:11b, where they are linearly spaced. The global trend is the same in both plots, where around 1 MeV, the efficiencies drop sharply and plateau towards 0. However, the logarithmically spaced thresholds reveal a second plateau considerably earlier in the energy threshold region. This could yield information regarding the noise drop-off region, but a more rigorous analysis must be made in order to be conclusive.

In figure Fig:12, the measured data intersects the simulated coincidences seemingly in a range between 0.6 and 1 MeV. However, upon factoring in sensitivity, the intersection points, as shown in figure fig:13, group together more closely to 1.2 MeV. This gave a first estimate of the energy to tension conversion, as the discriminator thresholds were all set to -150 mV for this measurement. The coincidence logics used as well as their counts as a function of energy threshold are plotted in figure Fig:14a. The trend shown in this plot is that the logics with the most channels implemented seem to have more counts, with the only exception being channel 1 on its own. As such, the configurations consisting of channel 1 and channel 1 and all the others were considered. The figure Fig:14b shows the intersections of the measured data normalized to channel 1 with the coincidence curve for the logic  $(ch1 \wedge (ch2 \vee \dots \vee ch8))$ . With the intersections, the mean was calculated as well as the standard deviation. When plotting a vertical axis at the mean value, the intersection between this line and the non normalized coincidence curve gives an estimate of the efficiency. Using the standard deviation, it is possible to estimate the uncertainty in this obtained value. For the 2 channel logics plotted in figures Fig:15b (channel 1), and Fig:15a (channel 1 and .....), the corresponding efficiencies are respectively  $(16 \pm 2)\%$  and  $(13 \pm 3)\%$ .

The results from the positron measurements, shown in figure Fig:16, do not seem to reveal a photopeak. Given that when positrons annihilate with electrons, they emit a 511 keV photon, it is expected that for some threshold tension range, there would be a plateau, and finally a drop-off at the voltage corresponding to an energy of 511 keV. This is absent in the previous

figure. However, using equation eq:2 and the results from this plot, it is possible to calculate the sensitivity ratio and calibrate the coincidence counting process. Moreover, the photopeak is absent from the Fluka simulations as well, as can be observed in figure Fig:17a. The suspected reason for this is that the scintillating bar is not thick enough for a 511 keV  $\gamma$  to fully deposit all of its energy. This hypothesis is reinforced by the fact that when simulating a thicker scintillating bar, the expected plateau appears, albeit faintly, as can be seen in figure Fig:17b. A related issue is the apparent disagreement between the energy thresholds for the two measurements, antiprotons and positrons. The threshold value we chose, -150 mV, corresponds to about 1.2 MeV according to our analysis of antiproton data. Yet we clearly see counts in the positron data at this threshold, even though the gamma rays must deposit less than 511 keV. This apparent discrepancy may be due to the different conversion efficiency (energy to optical photons) for the different particles produced in the annihilation of antiprotons vs. positrons [6].

## 5 Conclusion

The MCP and SiPM detector system was studied. The noise picked up by the slow SiPM was analyzed, and given an acceptable threshold, the counts from the slow SiPM were compared to those of the fast SiPM. This gave a preliminary estimate of the counting efficiency of the fast SiPM, assuming the slow SiPM was 100% effective. The discriminated signal of the fast SiPM was compared to the linear signal of the fast SiPM, where the intersections between the two seemingly agreed with the actual discriminator threshold. Next, the scintillating bar system was studied: first with the help of FLUKA simulations antiprotons, then with measured data, and finally with data from positron simulations and measurements. The Intersections of the measured data with the simulated data gave a preliminary energy threshold, from which the efficiency of the system could be estimated. This process was further refined using the positron data, which enabled the sensitivity of each channel to be quantified. The studies strongly suggest the presence of between 1.0 and 1.5 million antiprotons in the Cusp trap. The AMT scintillator has not been sufficiently well characterized for a more precise determination. There remain several points that must be addressed, such as the validity of the uncertainty in the SiPM analysis, as well as the uncertainty in the scintillating bar analysis, or the missing photopeak for positron data. These are interesting points for further analysis of this experiment.

## References

- [1] S. Maury, *The antiproton decelerator: AD*, Hyperfine Interactions 109 (1997), pp. 43–52.
- [2] M. Hori and J. Walz, *Physics at CERN’s antiproton decelerator*, Progress in Particle and Nuclear Physics 72 (2013), pp. 206–253.
- [3] E. Hunter, J. Fajans, N. Lewis, A. Povilus, C. Sierra, C. So, and D. Zimmer, *Plasma temperature measurement with a silicon photomultiplier (SiPM)*, Review of Scientific Instruments 91 (2020).
- [4] B. Radics, Y. Nagata, Y. Yamazaki, S. Ishikawa, N. Kuroda, Y. Matsuda, M. Anfreville, S. Aune, M. Boyer, F. Chateau, *et al.*, *The ASACUSA micromegas tracker: A cylindrical, bulk micromegas detector for antimatter research*, Review of Scientific Instruments 86 (2015).
- [5] G. Battistoni, T. Boehlen, F. Cerutti, P.W. Chin, L.S. Esposito, A. Fasso, A. Ferrari, A. Lechner, A. Empl, A. Mairani, *et al.*, *Overview of the FLUKA code*, Annals of Nuclear Energy 82 (2015), pp. 10–18.

- [6] S. Mukhopadhyay, *Plastic gamma sensors: an application in detection of radioisotopes*, in *Hard X-Ray and Gamma-Ray Detector Physics V*, Vol. 5198. SPIE, 2004, pp. 62–72.

## 6 Appendix

**AMT  $\bar{p}$  estimate** To estimate the amount of  $\bar{p}$  counted by the AMT system as well as the uncertainty, the following measurements were used:

Table 2: Counted annihilations when dumping  $\bar{p}$  to the field null.

	AMT ch1	AMT coincidence
run 1	$1.61 \cdot 10^5$	$1.28 \cdot 10^5$
run 2	$1.55 \cdot 10^5$	$1.23 \cdot 10^5$
run 3	$1.58 \cdot 10^5$	$1.26 \cdot 10^5$

and the following formula was used:

$$\frac{\sigma}{\eta} + \frac{\bar{X} \cdot \Delta\eta}{\eta^2} \quad (3)$$

with  $\sigma$  the standard deviation of the measurements,  $\eta$  the coincidence counting efficiency of the configuration,  $\bar{X}$  the mean of the measurements, and  $\Delta\eta$  the uncertainty in the efficiency for the given configuration.

**Sensitivity** We are not within reasonable certainty that the sensitivity was corrected the right way. Here is another graph like figures Fig:12 and Fig:13, with the sensitivity inverted.

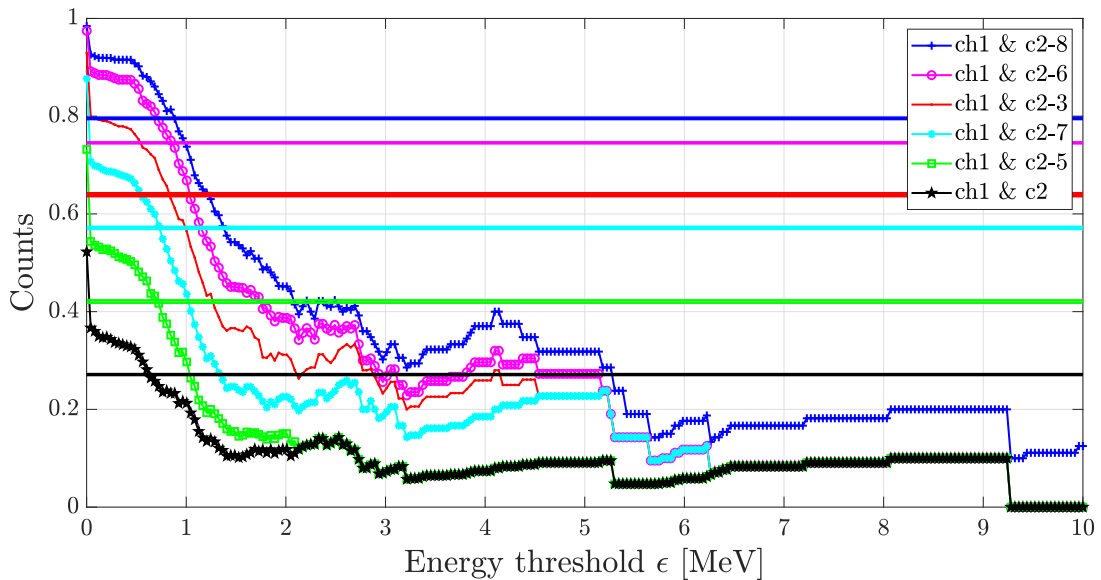


Figure 18: Simulated coincidence logic counts normalized to the counts from channel 1 with measured data, as well as simulated data corrected for sensitivity (take inverse of eq:2).